

X-RAY EMISSION FROM THE DOUBLE-BINARY OB-STAR SYSTEM QZ CAR (HD 93206)

E. R. PARKIN^{1,2}, P. S. BROOS³, L. K. TOWNSLEY³, J. M. PITTARD², A. F. J. MOFFAT⁴, Y. NAZÉ¹, G. RAUW¹,
L. M. OSKINOVA⁵, AND W. L. WALDRON⁶

¹ Institut d'Astrophysique et de Géophysique, Université de Liège, 17, Allée du 6 Août, B5c, B-4000 Sart Tilman, Belgium; parkin@mso.anu.edu.au

² School of Physics and Astronomy, The University of Leeds, Woodhouse Lane, Leeds LS2 9JT, UK

³ Department of Astronomy and Astrophysics, Pennsylvania State University, 525 Davey Laboratory, University Park, PA 16802, USA

⁴ Département de Physique, Université de Montréal, C.P. 6128, Succ. Centre-Ville, Montréal, QC H3C 3J7, Canada

⁵ Institute for Physics and Astronomy, University of Potsdam, 14476 Potsdam, Germany

⁶ Eureka Scientific Inc., 2452 Delmer Street, Oakland, CA 94602, USA

Received 2010 November 1; accepted 2010 December 22; published 2011 April 28

ABSTRACT

X-ray observations of the double-binary OB-star system QZ Car (HD 93206) obtained with the *Chandra X-ray Observatory* over a period of roughly 2 years are presented. The respective orbits of systems A (O9.7 I+b2 v, $P_A = 21$ days) and B (O8 III+o9 v, $P_B = 6$ days) are reasonably well sampled by the observations, allowing the origin of the X-ray emission to be examined in detail. The X-ray spectra can be well fitted by an attenuated three-temperature thermal plasma model, characterized by cool, moderate, and hot plasma components at $kT \simeq 0.2, 0.7,$ and 2 keV, respectively, and a circumstellar absorption of $\simeq 0.2 \times 10^{22} \text{ cm}^{-2}$. Although the hot plasma component could be indicating the presence of wind–wind collision shocks in the system, the model fluxes calculated from spectral fits, with an average value of $\simeq 7 \times 10^{-13} \text{ erg s}^{-1} \text{ cm}^{-2}$, do not show a clear correlation with the orbits of the two constituent binaries. A semi-analytical model of QZ Car reveals that a stable momentum balance may not be established in either system A or B. Yet, despite this, system B is expected to produce an observed X-ray flux well in excess of the observations. If one considers the wind of the O8 III star to be disrupted by mass transfer, the model and observations are in far better agreement, which lends support to the previous suggestion of mass transfer in the O8 III + o9 v binary. We conclude that the X-ray emission from QZ Car can be reasonably well accounted for by a combination of contributions mainly from the single stars and the mutual wind–wind collision between systems A and B.

Key words: hydrodynamics – stars: early-type – stars: individual (QZ Carinae) – stars: massive – stars: winds, outflows – X-rays: stars

Online-only material: color figure

1. INTRODUCTION

Residing within the Great Carina Nebula at a distance of 2.3 kpc (Allen & Hillier 1993; Walborn 1995; Smith 2002—see also Smith 2006), the multiple star system QZ Car (HD 93206) is the brightest object in the Collinder 228 star cluster, in the older southern part of the Nebula. Via independent observations, the presence of two systems of periodically variable lines in the spectrum led Leung et al. (1979) and Morrison & Conti (1979) to conclude that there were four stars present, where the period of the stronger line variability was due to the ~ 20 day binary (hereafter system A) and the period of the weaker lines corresponding to the ~ 6 day period eclipsing binary (hereafter system B). Despite this great success, two of the components of the system remain undetected. The mass functions derived for the separate binary systems suggest that the eclipsing binary component with undetected lines is more massive than its binary companion, whereas in the longer period, non-eclipsing binary the unseen companion is a few times smaller than the primary component and therefore most likely has unobservable lines. A schematic of QZ Car is shown in Figure 1 and system and stellar parameters are noted in Tables 1 and 2, respectively. Based on the Roche-lobe filling factors,⁷ Leung et al. (1979) suggested that the stars in system B have undergone some mass exchange. Morrison & Conti (1980) also noted that there is

evidence of substantial mass loss from the primary star in system B due to a systematic difference in velocity between He I and Si IV, which from an evolutionary point of view makes it the most interesting star in this system.

Little is known about the mutual orbit of systems A and B. The results of Leung et al. (1979) and Morrison & Conti (1980) were in agreement that the orbital period of the super-binary must be $\lesssim 25$ yr. Yet, this was based on the assumption that at the time of their observations the system was at quadrature, or apastron in an eccentric orbit. The speckle observations of Mason et al. (1998) were unsuccessful in spatially resolving the components of HD 93206, as were the more sensitive FGS1r observations of Nelan et al. (2004). Therefore, the non-resolution of the system places an upper limit of $\simeq 35$ AU on the projected separation of the two binary systems.

In this paper, we report on the recent detection of X-ray emission from QZ Car. For single massive stars, it is widely accepted that (soft) X-ray emission is generated by embedded wind shocks (EWSs) which are produced by the inherent instability of the line-driving mechanism (e.g., Owocki et al. 1988). Early X-ray observations of massive stars in binary systems revealed them to be overluminous compared with the expected cumulative luminosity of the separate stars (Pollock 1987; Chlebowski & Garmany 1991).⁸ The additional

⁷ The parameters in Table 2 give Roche-lobe filling factors for stars B1 and B2 of $\simeq 1.0$ and 0.4 , respectively.

⁸ More recent results (Oskinova 2005; Nazé 2009; Nazé et al. 2011) suggest that only prominent colliding winds binary systems are significantly overluminous in X-rays.

Table 1
System Parameters for QZ Car

System	Components	P	a (R_{\odot})	e	ω ($^{\circ}$)	i ($^{\circ}$)
A	A1+A2	20.72 days	116	0.34	141	60
B	B1+B2	5.999 days	49	0.1	$\simeq 20$	86
AB	A+B	$\lesssim 25.4$ yr	$\lesssim 8687$	0.0	0	60

Notes. P is the period of the orbit, a is the semimajor axis of the orbit, e is the orbital eccentricity, ω is the longitude of periastron, and i is the inclination angle of the orbital plane (measured against the pole). Orbital periods are taken from Mayer et al. (2001), e 's and ω 's from Morrison & Conti (1980), and i 's from Leung et al. (1979). For system AB the projected semimajor axis is quoted. We note that $e = 0.0$ is only a preliminary assumption for system AB, and such long-period systems can in fact have $0.000 \lesssim e \lesssim 0.999$.

luminosity in this case is the result of wind–wind collision shocks (e.g., Stevens et al. 1992; Pittard & Stevens 1997; Parkin & Pittard 2008). For QZ Car, further additional X-ray emission may be contributed by the mutual wind–wind collision between the two binary systems (MWC). The observed flux may therefore be a complex cocktail of X-ray emission from different sources, and disentangling its origin(s) is not straightforward. We note that the central multiple star system is surrounded by a subcluster of faint X-ray emitting pre-main-sequence stars, for which we refer the reader to Townsley et al. (2011) for a detailed analysis.

The X-ray observations of QZ Car were obtained with the *Chandra X-ray Observatory* (hereafter *Chandra*) as part of the Chandra Carina Complex Project (CCCP; Townsley et al. 2011; Broos et al. 2011). The X-ray spectra can be reasonably well fitted by three-temperature plasma models with a hot component at $\simeq 2$ keV. This, combined with the fact that the observed fluxes appear to be overluminous in comparison to the total X-ray emission expected from the single stars, may be indicating the presence of shock heated plasma from wind–wind collisions. However, attempts to match the best-fit parameters from the spectral fits to the periods of either system A or B do not reveal any strong correlation. To aid in the interpretation of the observations a semi-analytical model is constructed which indicates that although normal wind–wind collision shocks are not expected, unless the wind of the O8 III star is suppressed the model overpredicts the observed X-ray emission by a factor of ~ 10 – 20 . The suppressant in this case could be mass transfer

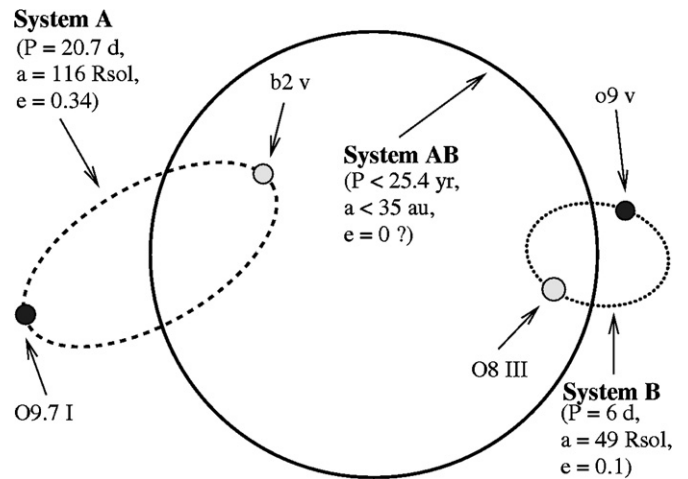


Figure 1. Schematic diagram of the multiple star system QZ Car. For further details see Tables 1 and 2. For system AB the projected semimajor axis is quoted. Note that this schematic is not to scale.

(A color version of this figure is available in the online journal.)

from the O8 III star (Leung et al. 1979). We conclude that the dominant contributions to the observed X-ray flux are the single stars and the MWC. The remainder of this paper is structured as follows: in Section 2 we present the observations, Section 3 describes the results from spectral fitting, Section 4 details a semi-analytical model of QZ Car. The results from this work are discussed in Section 5, and we close with a summary of our conclusions in Section 6.

2. OBSERVATIONS

A total of nine observations over a period of roughly two years, and combining relatively on-axis and far off-axis exposures taken with both the I array and the S array, have been obtained for QZ Car (Table 3). Due to the brightness of the central source the I-array observation (ObsID 9482) was affected by photon pile-up, which we account for in our analysis (see Section 3). The I-array observation alone would have provided a single snapshot of QZ Car; however, during the CCCP QZ Car has been observed by the S-array CCDs on eight separate occasions, and in some cases with a considerable exposure time (e.g., 88 ks for ObsID 6402). Fortunately for the current investigation this considerably expands the available data set.

Table 2
Stellar Parameters for QZ Car

Component	Sp. Type	T_{eff} (K)	R_* (R_{\odot})	M_* (M_{\odot})	L_* ($\log[L_*/L_{\odot}]$)	\dot{M} ($M_{\odot} \text{ yr}^{-1}$)	v_{∞} (km s^{-1})
A1	O9.7 I	32000	22.5	40	5.7	2.2×10^{-6}	2140
A2	b2 v	20000	6.0	10	3.7	2.4×10^{-9}	1040
B1	O8 III	32573	26.9	14.1	5.3	5.2×10^{-7}	2220
B2	o9 v	32463	8.9	28	4.9	6.4×10^{-8}	2850

Notes. For consistency we adopt the labeling of Mayer et al. (2001) for the system components. The spectral types for components A1 and B1 were determined from observations by the OWN Team (R. Barbá 2010, private communication). The values of T_{eff} , R_* , and M_* for components A1 and B2 are taken from Leung et al. (1979), for component B1 values were taken from Martins et al. (2005), and for component A2 the respective values have been estimated by a comparison to objects of similar spectral type in Prinja (1989). The values of v_{∞} are calculated as $2.6v_{\text{esc}}$ for components A1, B1, and B2, and as $1.3v_{\text{esc}}$ for component A2 (based on T_{eff}), where $v_{\text{esc}} = \sqrt{2GM_*/R_*}$. The \dot{M} values are calculated using the cooking recipe from Vink et al. (2000). We note that the spectral types of components A2 and B2 are not based on true spectral classifications (i.e., direct detection in the optical spectrum), and are in fact based on photometric and/or color information. Therefore, we use lowercase letters to denote the spectral type of components A2 and B2.

Table 3
Summary of the Observations

ObsID	CCD	θ ($^{\circ}$)	Date	T (ks)	R (ks $^{-1}$)	ϕ_A	ϕ_B
6402	S2	16.01	2006 Aug 30	87	76.5	0.10	0.07
9492	S3	14.04	2008 Feb 12	20	119.0	0.68	0.50
9816	S3	14.04	2008 Feb 15	21	138.5	0.81	0.94
9493	S2	17.23	2008 Feb 25	20	83.1	0.32	0.70
9830	S2	17.23	2008 Feb 28	20	73.3	0.45	0.14
9831	S2	17.23	2008 Mar 1	16	78.4	0.52	0.41
9498	S3	18.94	2008 May 24	32	118.3	0.61	0.53
9859	S3	18.94	2008 May 31	28	129.4	0.91	0.57
9482	I3	3.41	2008 Aug 18	57	73.3	0.75	0.83

Notes. ϕ_A and ϕ_B are the corresponding orbital phases for systems A and B, respectively, calculated using the ephemerides of Mayer et al. (2001). The time of periastron used for system A is taken as JD 2442530.49, which refines the time of periastron determined by Morrison & Conti (1980) using the more recent observations of Mayer et al. (2001). For system B, the ephemeris is extrapolated from the minimum observed by Mayer et al. (1998) at JD 2448687.16. θ is the off-axis angle, T is the exposure time, and R is the count rate for each observation. The CCCP ACIS source label and official source name for QZ Car are C2_1111 and 104422.91–595935.9, respectively.

Source and spectrum extraction were performed using ACIS EXTRACT (Broos et al. 2002, 2007, 2010; Townsley et al. 2006), an IDL-based package developed for processing ACIS data. For each observation, a background spectrum was taken from an annulus around QZ Car, and the resulting background subtracted source spectrum was binned to achieve a signal-to-noise ratio of 3. Note that the far off-axis (ACIS-S) extractions of QZ Car encompass a nearby subcluster of low-mass stars. However, these potential contaminants to the off-axis QZ Car spectra are very weak when resolved in the on-axis observation, and the off-axis extractions show no indication of a large flare from one of these companions: (1) the median energy shows relatively minor changes and (2) Kolmogorov–Smirnov tests on the individual light curves do not reveal any considerable evidence for variability.

3. RESULTS

The 0.5–8 keV spectra were fitted using v12.5.1 of XSPEC⁹ (Arnaud 1996). To model the emission we use the *apec* thermal plasma model for collisionally ionized gas (Smith et al. 2001), and to account for attenuation we adopted the *tbabs* photoelectric absorption model (see Wilms et al. 2000). In all calculations the abundances were kept fixed at the solar values (Anders & Grevesse 1989). To fit the spectra we use a three-temperature combination, $tbabs_{ISM} \times tbabs(apec+apec+apec)$, with an interstellar medium (ISM) absorption component, $tbabs_{ISM}$, fixed at $0.35 \times 10^{22} \text{ cm}^{-2}$ (Povich et al. 2011). By separating the column into ISM and circumstellar components we gain more information about variations in the local absorption, which is a particularly useful approach when studying the wind–wind collision in binary systems (e.g., De Becker et al. 2005; Pittard & Parkin 2011). Similarly, the separate emission components can be used to search for correlations with the components of the system (i.e., EWSs, wind–wind collision regions (WCRs) and the MWC). The physical interpretation of the adopted model combination assumes that the circumstellar absorption to all

emission components is the same.¹⁰ As noted in Section 2, ObsID 9482 was affected by photon pile-up¹¹, which we correct for using an additional pileup model (Davis 2001). The pileup parameter *fr_time* was frozen to 3.31 s to account for exposure time discarded during the standard data cleaning process¹²; the best-fit values for the thawed α and *psfrac* parameters were found to be 0.954 and 0.633.

A visual inspection of the spectra shows that a three-temperature thermal plasma model provides a reasonably good fit to the data (Figure 2). In general there is a cool component at $kT_1 \simeq 0.2$ keV, a moderate temperature component at $kT_2 \simeq 0.7$ keV, a hot component at $kT_3 \simeq 2$ keV, a column density, $N_H \simeq 0.2 \times 10^{22} \text{ cm}^{-2}$, and a 0.5–8 keV flux $\simeq 7 \times 10^{-13} \text{ erg s}^{-1} \text{ cm}^{-2}$. Comparing these results to those for QZ Car in Nazé et al. (2011), we see that there is agreement in the circumstellar column and in the presence of a moderate temperature component at $\simeq 0.7$ keV. However, the derived flux and temperature of the hotter plasma component are notably higher in this work. These differences are likely due to the use of three-temperature fits in this work, whereas Nazé et al. apply a two-temperature fit.¹³ We note that two-temperature fits were also examined, however, statistically better results could be attained for all observations using three-temperature spectral fits. For example, for ObsID 6402, the reduced chi-squared attained from two-temperature and three-temperature fits were 1.84 and 1.33, respectively. In both cases, the highest temperature component was at $kT \simeq 2.1$ keV. The higher chi-squared in the case of the two-temperature model was due to poorer fit to the spectrum at energies $\lesssim 1$ keV. Adding the third temperature component significantly remedied this.

From the best-fit parameters in Table 4 (see also Figure 3), one sees that kT_1 and kT_2 appear to be reasonably well constrained. However, in contrast kT_3 and N_H do not. Recalling that N_H is intended to account for the circumstellar absorption to potentially numerous regions of X-ray emitting plasma, this is unsurprising. Despite this, using the conversion factor of $N_H = A_v \times (1.9 \times 10^{21}) \text{ cm}^{-2}$ (e.g., Cox 2000), there is good agreement with the visual extinction from the observed color indices ($A_v = 1.2$ mag; Herbst 1976; Leung et al. 1979). Comparisons of the X-ray spectra of QZ Car against two-temperature fits to single and binary stars of similar spectral type in Carina (Nazé et al. 2011) are inconclusive in so much as they do not directly support/rule-out the presence of wind–wind collision shocks based solely on the spectral shape and the derived plasma temperatures (i.e., the presence of a hot component with $kT \gtrsim 1$ keV).

Examining the variation of the best-fit parameters plotted against the orbital phases of the binary systems we see that both kT_1 and kT_2 remain relatively constant across all observations (Figure 3). A tentative correlation between kT_3 and system A could be suggested although the errors are quite large (due to

¹⁰ A more physically meaningful model combination would incorporate separate absorption components for each emission component (i.e., spatially distinct emission regions). However, due to limited statistics attempts to fit the spectra with such a model combination were unsuccessful.

¹¹ http://cxc.harvard.edu/ciao/why/pileup_intro.html

¹² The Chandra ABC Guide to Pileup (http://cxc.harvard.edu/ciao/download/doc/pileup_abc.pdf) describes the correction to *fr_time* that is required for all ACIS sources.

¹³ The quality of the data constrains the complexity of the model that can be applied in spectral fitting. Nazé et al. (2011) adopted two-temperature model fits to perform a consistent analysis of the entire OB star sample from the CCCP, which consists of data of varying quality. In the present paper, we aim to perform a more detailed analysis of QZ Car, for which the data are of sufficient quality to permit meaningful results from the use of a three-temperature model.

⁹ <http://heasarc.gsfc.nasa.gov/docs/xanadu/xspec/>

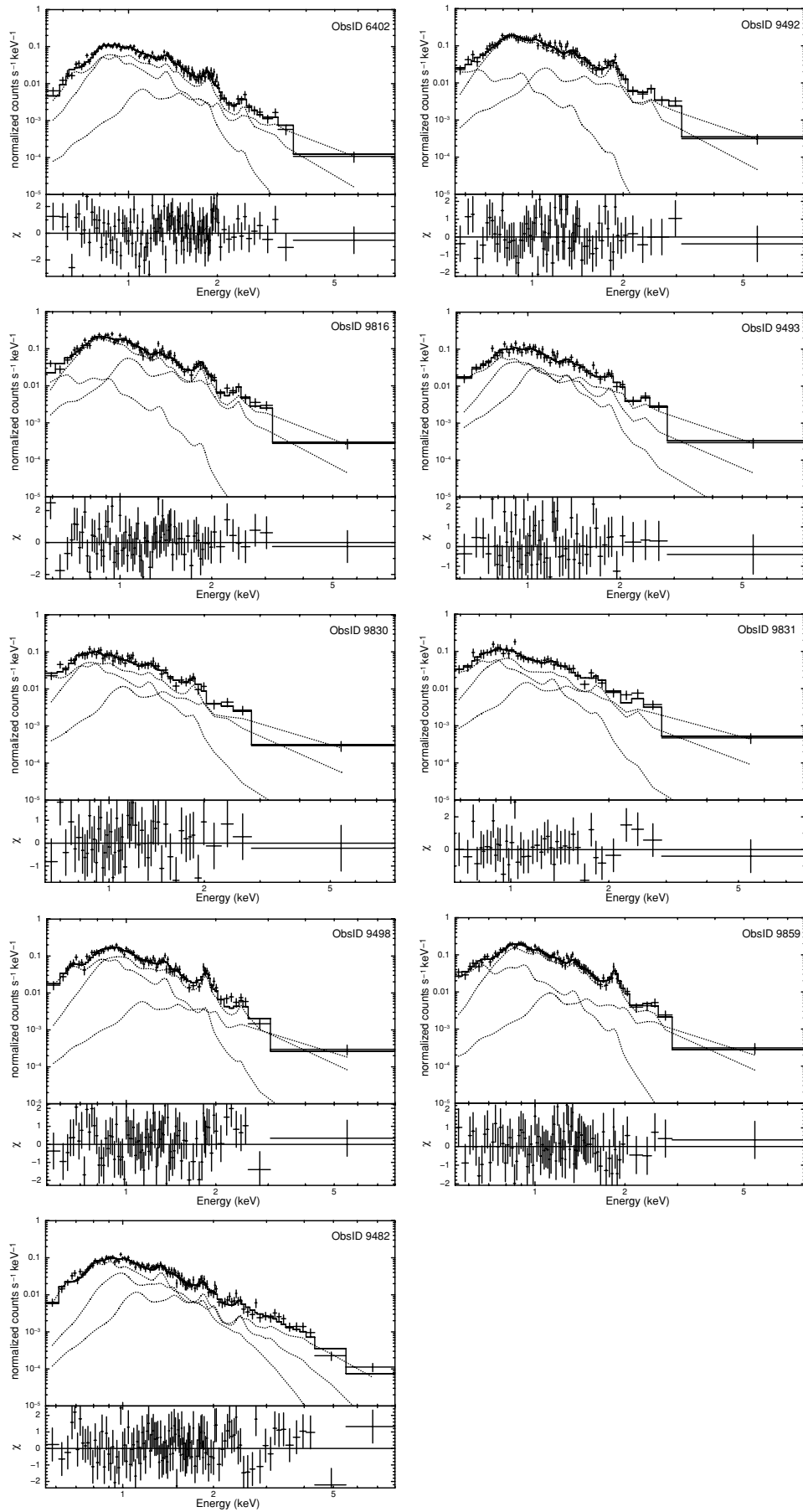


Figure 2. 0.5–8 keV X-ray spectra of QZ Car with best-fit models attained with the combination $tbabs_{\text{ISM}} \times tbabs(apec + apec + apec)$.

Table 4
Results from Spectral Fitting

ObsID	N_{H} (10^{22} cm^{-2})	kT_1 (keV)	Norm ₁ (10^{-4} cm^{-5})	kT_2 (keV)	Norm ₂ (10^{-4} cm^{-5})	kT_3 (keV)	Norm ₃ (10^{-4} cm^{-5})	0.5–8 keV flux ($10^{-13} \text{ erg cm}^{-2} \text{ s}^{-1}$)	χ^2 (d.o.f)
6402	0.25 $^{0.05}_{0.05}$	0.26 $^{0.05}_{0.06}$	23.4 $^{12.9}_{8.4}$	0.60 $^{0.12}_{0.04}$	7.22 $^{3.06}_{3.82}$	2.10 $^{1.12}_{0.46}$	1.32 $^{0.45}_{0.49}$	6.55	1.33 (102)
9492	0.20 $^{0.09}_{0.10}$	0.15 $^{0.05}_{0.06}$	24.3 $^{94.8}_{18.3}$	0.58 $^{0.03}_{0.03}$	9.71 $^{2.42}_{2.80}$	1.90 $^{1.12}_{0.40}$	2.52 $^{0.78}_{0.93}$	7.09	0.96 (68)
9816	0.12 $^{0.08}_{0.08}$	0.20 ^{fr}	5.46 $^{7.08}_{3.74}$	0.61 $^{0.04}_{0.03}$	7.73 $^{2.24}_{1.16}$	1.49 $^{0.20}_{0.23}$	3.32 $^{0.62}_{0.72}$	7.70	1.00 (74)
9493	0.16 $^{0.14}_{0.15}$	0.28 $^{0.07}_{0.08}$	15.0 $^{27.0}_{11.1}$	0.69 $^{0.31}_{0.12}$	3.37 $^{5.33}_{2.11}$	1.49 $^{0.47}_{0.26}$	3.20 $^{1.05}_{1.21}$	7.00	0.97 (52)
9830	0.24 $^{0.15}_{0.17}$	0.23 $^{0.08}_{0.08}$	26.8 $^{88.8}_{20.2}$	0.62 $^{0.15}_{0.10}$	5.81 $^{5.05}_{4.10}$	1.94 $^{2.92}_{0.48}$	1.96 $^{1.02}_{0.99}$	6.19	0.76 (47)
9831	0.19 $^{0.21}_{0.19}$	0.23 $^{0.13}_{0.23}$	27.0 $^{160}_{24.2}$	0.79 $^{0.25}_{0.17}$	4.57 $^{4.20}_{2.22}$	2.37 $^{4.65}_{0.80}$	2.80 $^{1.22}_{1.40}$	7.84	0.94 (36)
9498	0.27 $^{0.09}_{0.08}$	0.23 $^{0.03}_{0.05}$	34.9 $^{32.3}_{15.9}$	0.71 $^{0.05}_{0.10}$	7.16 $^{4.28}_{1.85}$	2.63 $^{-}_{1.3}$	1.05 $^{0.87}_{0.74}$	7.14	1.14 (78)
9859	0.22 $^{0.10}_{0.09}$	0.18 $^{0.06}_{0.04}$	42.3 $^{45.3}_{22.1}$	0.58 $^{0.03}_{0.03}$	10.8 $^{2.97}_{4.36}$	2.14 $^{-}_{0.76}$	1.32 $^{0.76}_{0.67}$	7.78	0.77 (76)
9482	0.31 $^{0.06}_{0.08}$	0.26 $^{0.03}_{0.03}$	31.3 $^{26.8}_{16.1}$	0.81 $^{0.13}_{0.11}$	2.66 $^{2.80}_{0.85}$	1.96 $^{0.35}_{0.31}$	1.63 $^{0.11}_{0.81}$	5.28	1.03 (106)
Average	0.22	0.22	25.6	0.67	6.56	2.00	2.12	6.95	0.99

Notes. The “fr” indicates that the parameter was frozen at this value during spectral fitting. The 90% confidence level errors are quoted with a hyphen corresponding to an unconstrained error.

limited statistics in the spectra at higher energies) and one could equally favor a null result. Additionally, an increase in N_{H} would be expected as higher temperature plasma close to the apex of the WCR(s) comes into view, which is not seen in the fits. Finally, we note that the 0.5–8 keV fluxes calculated from the spectral fits do not show any clear correlation with the orbit of either system A or B.

4. A MODEL OF QZ CAR

The results of the analysis so far do not highlight any obvious link between the observed X-ray emission and the orbit of either binary. However, with potentially multiple sources of X-rays it is possible that any signature of the orbit may be smeared-out in the cumulative emission. To better constrain the roles of the various components of the system, and their contribution to the total emission, we now construct a semi-analytical model of QZ Car.

4.1. Intrinsic X-ray Emission

First, we estimate the contribution to the X-ray luminosity from EWSs using the canonical relation $L_X = 10^{-7} L_{\text{bol}}$, which amounts to a flux of $\simeq 4.4 \times 10^{-13} \text{ erg s}^{-1} \text{ cm}^{-2}$. Then, following Pittard & Stevens (2002), we can estimate the X-ray flux from the wind–wind collisions using the simple relation:

$$f_{\text{Xi}} = \frac{1}{8\pi D^2} \dot{M}_i v_i^2 \frac{\Xi_i}{\chi_i}, \quad (1)$$

where D is the distance to QZ Car (taken to be 2.3 kpc), Ξ is the fractional wind kinetic power normal to the contact discontinuity, χ is the cooling parameter ($= v_8^4 d_{12} / \dot{M}_{-7}$, see Stevens et al. 1992), and the subscript i denotes the contributing component. The parameter Ξ is dependent on the wind momentum ratio of the system, $\eta_{ij} = (\dot{M}_j v_j) / (\dot{M}_i v_i)$, where the subscript j denotes the component index of the binary companion. For $\eta_{ij} = (0.01, 0.1, 1.0)$, $\Xi_i = (0.0042, 0.033, 0.167)$ and $\Xi_j = (0.564, 0.403, 0.167)$, i.e., the value of Ξ is higher for the weaker wind because a greater fraction of that wind collides close to the shock normal. The parameter χ is the ratio of the characteristic flow time to the cooling time; if $\chi \lesssim 1$ the post-shock gas is radiative, whereas if $\chi \gg 1$ the post-shock gas is adiabatic. Note that in the case where $\chi < 1$ we set $\chi = 1$ to satisfy energy conservation.

In systems A and B the separation of the stars is relatively small, and the stellar winds may not have reached their terminal velocities. This has consequences for the position of the momentum balance surface between the stars (if one exists). If we assume that the wind velocity follows a β -velocity law (i.e., $v(r) = v_\infty(1 - R_*/r)^\beta$), and set $\beta = 1$ for simplicity, we can calculate the position of the momentum balance point by numerical solution of the following equation for the distance from star i to the momentum balance point (along the lines of center), r ,

$$\frac{\dot{M}_i v_{\infty i}}{r^2} \left(1 - \frac{R_{*i}}{r}\right) = \frac{\dot{M}_j v_{\infty j}}{(d_{\text{sep}} - r)^2} \left(1 - \frac{R_{*j}}{d_{\text{sep}} - r}\right). \quad (2)$$

It is then straightforward to calculate the effective values of η , Ξ , χ , and f_{Xi} from the shocked gas of each wind, where the pre-shock wind speed along the lines of center rather than the terminal wind speed is used in the calculations. The distance from the star to the shock rather than the binary separation is used to calculate χ .

We can repeat this process for the MWC. For this purpose, we approximate the mass-loss rates and terminal wind speeds for systems A and B as

$$\dot{M}_A = \dot{M}_{A1} + \dot{M}_{A2}, \quad (3)$$

$$\dot{M}_B = \dot{M}_{B1} + \dot{M}_{B2}, \quad (4)$$

$$v_A = \left(\frac{\dot{M}_{A1} v_{A1}^2 + \dot{M}_{A2} v_{A2}^2}{\dot{M}_{A1} + \dot{M}_{A2}} \right)^{1/2}, \quad (5)$$

$$v_B = \left(\frac{\dot{M}_{B1} v_{B1}^2 + \dot{M}_{B2} v_{B2}^2}{\dot{M}_{B1} + \dot{M}_{B2}} \right)^{1/2}. \quad (6)$$

Parameter values pertaining to the X-ray emission calculations for the MWC are listed in Table 5. We note that Equations (3)–(6) should provide a reasonable approximation as, due to the relatively large separation of system AB, the stellar winds should have had sufficient time to mix.

At all orbital phases in systems A and B a wind–wind momentum balance does not occur and the wind of the weaker star

Table 5

Parameters for the Mutual Wind–Wind Collision between Systems A and B

Parameter	System A	System B
\dot{M} (M_{\odot} yr $^{-1}$)	2.2×10^{-6}	5.8×10^{-7}
v_{∞} (cm s $^{-1}$)	2.14×10^8	2.30×10^8
Ξ	0.06	0.35
χ	570	2860
f_X (10^{-13} erg s $^{-1}$ cm $^{-2}$)	5.3	1.9
η		0.28
$d_{\text{sep(A+B)}}$ (10^{12} cm)		600
N_{H} (cm $^{-2}$)		1.3×10^{20}

Notes. The values of f_X and N_{H} are calculated from Equations (1) and (8), respectively. The values of Ξ for systems A and B were interpolated from the results of Pittard & Stevens (2002) for the respective values of η .

is completely crushed by the stronger opponent.¹⁴ Therefore, the values of Ξ_{A2} and Ξ_{B2} are set to zero (i.e., no contribution to the X-ray emission) and Ξ_{A1} and Ξ_{B1} are instead approximated as the fractional solid angle subtended by the face of their respective companion star,

$$\Xi_i = \frac{1}{4\pi} \left(1 - \cos \left\{ \tan^{-1} \left(\frac{R_{*j}}{d_{\text{sepi-j}}} \right) \right\} \right). \quad (7)$$

Figure 4 shows the variation of the pre-shock velocities, χ 's, Ξ 's, and kT with orbital phase. Note that, to avoid confusion with references to the intrinsic emission from the individual stars, the characteristics of component A1's wind colliding against its opposing star (component A2) is referred to as component A1-O. The same nomenclature is adopted for component B1. The characteristic energy of the emitted X-rays is given by $kT \simeq 1.17v_8^2$ keV, where v_8 is the pre-shock velocity in units of 10^8 cm s $^{-1}$. For now, the pre-shock velocities of component B1-O are calculated assuming that it drives a wind towards its binary companion, rather than the system being semi-detached. Later (Section 4.3), we consider the possibility of zero colliding winds emission from system B.

Evidently, terminal wind speeds are not reached prior to collision (see Table 2). The cooling parameters, χ 's, for components A1-O and B1-O are sufficiently high for the post-shock gas to be adiabatic at phases close to apastron, whereas they may become radiative ($\chi \lesssim 1$) around periastron. The value of Ξ for component B1-O is the highest at all orbital phases, representative of the larger fractional solid angle subtended by its companion star in comparison to component A1-O (see Equation (7)). The separation of systems A and B is sufficiently large that for the MWC the stellar winds will have reached their terminal velocities when they collide and this factor, combined with the low post-shock densities, leads to adiabatic shocks ($\chi_{\text{A}} = 570$ and $\chi_{\text{B}} = 2860$).

With a range of pre-shock velocities, the X-ray spectrum for QZ Car may well be dominated by emission from different shocked plasma components at different energies. Approximating the mean kT to be roughly half of the maximum value (to account for shock obliquity downstream from the apex of the WCR) we see that the predicted values for component A1-O (Figure 4(d)) are slightly lower than those derived for the hot

plasma component from the spectral fits (Figure 3 and Table 4) which has a mean temperature of 2.00 keV. In contrast, the mean temperatures from the MWC, where kT 's are $\simeq 2.7$ and 3.1 keV for system A and B, respectively, are higher than the observationally determined value. We note that all the values are higher than our adopted mean plasma temperature for EWSs of $kT = 0.25$ keV (e.g., Owocki & Cohen 1999).

The intrinsic X-ray flux from the individual shocked winds is shown in Figure 4(e). Component B1-O has the highest intrinsic X-ray luminosity, and so system B will dominate the X-ray emission if one assumes that the WCR has not been disrupted by mass transfer (for an alternative scenario see Section 4.3). Component A1-O is the *faintest* emitter (noting that component A1-O is bright for a brief period around periastron which is not sampled by our observations—see the ϕ_{A} 's in Table 3), followed by the EWSs ($\approx 4.4 \times 10^{-13}$ erg s $^{-1}$ cm $^{-2}$), both of which are fainter than the contribution from the MWC (Table 5). However, before making a detailed comparison with the best-fit values from the spectral fits we can improve our predictions by considering the energy dependence of the intrinsic and attenuated flux.

4.2. Attenuated Emission

The range of pre-shock velocities evident in Figure 4(a) will cause the spectra from the different components to have different characteristic energies. We can examine the implications of this energy dependence by first calculating an intrinsic spectrum at the mean post-shock gas temperature using the MEKAL plasma code (Kaastra 1992; Mewe et al. 1995), where solar abundances are assumed (Anders & Grevesse 1989). Each intrinsic spectrum is then scaled so that the integrated 0.5–8 keV fluxes are equal to the orbital phase dependent values, which for components A1-O and B1-O are shown in Figure 4(e). The top panel of Figure 5 shows the intrinsic spectra calculated for components A1-O, B1-O, the EWSs, and the MWC for ObsID 6402 (see Table 3 for the respective orbital phases of systems A and B). The EWSs clearly contribute the softest spectrum. For the wind–wind collision shocks, the lower pre-shock velocity for component B1-O relative to the MWC and component A1-O also results in a slightly softer spectrum. Interestingly, although not the brightest emitter, the MWC has the hardest spectrum.

To estimate the impact of circumstellar absorption, a characteristic column density for the binary systems can be calculated using Equation (11) from Stevens et al. (1992):

$$\bar{N}_{\text{H}} = 5 \times 10^{21} \frac{\dot{M}_{-7} (1 + \eta^{1/2})}{v_8 d_{12}}. \quad (8)$$

The expression for \bar{N}_{H} is for a binary system at quadrature where the winds are assumed to be at their terminal velocities (v_{∞} 's are used to calculate η in this case). When the stars are at quadrature all lines of sight to the emitting region will pass through the more powerful wind, which is assumed to be the dominant absorber. The orbital phase dependent characteristic column densities for systems A and B are $\simeq (4.9\text{--}9.9) \times 10^{21}$ cm $^{-2}$ and $\simeq (4.5\text{--}5.6) \times 10^{21}$ cm $^{-2}$, respectively. Note that in using Equation (8) we are essentially assuming the system is always at quadrature. To calculate the optical depth, we then multiply the total column density ($=\bar{N}_{\text{H}} + N_{\text{HISM}}$) by the opacity for gas at 10^4 K calculated using version c08.00 of Cloudy (Ferland 2000, see also Ferland et al. 1998), where solar abundances are assumed (Anders & Grevesse 1989). It is important to highlight that no circumstellar absorption is added for the EWSs as the L_X/L_{bol} relation is

¹⁴ The weaker star may radiatively brake the incoming wind, permitting a ram pressure balance (Gayley et al. 1997). This is unlikely to be effective for system A (due to the relatively low luminosity of component A2 compared to component A1) but may be effective in system B.

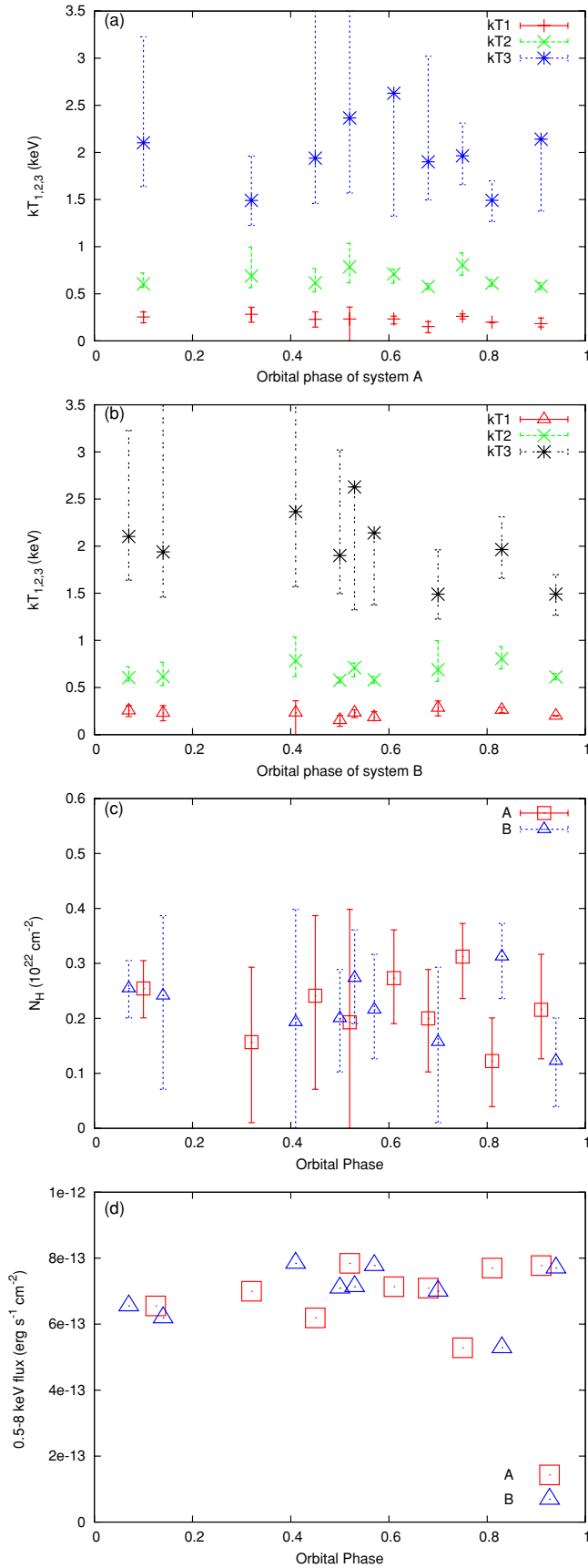


Figure 3. Optimal parameters attained from the spectral fits plotted against orbital phase for both systems A and B. From top to bottom: (a) kT 's for system A, (b) kT 's for system B, (c) N_H , and (d) the 0.5–8 keV flux. See also Table 4.

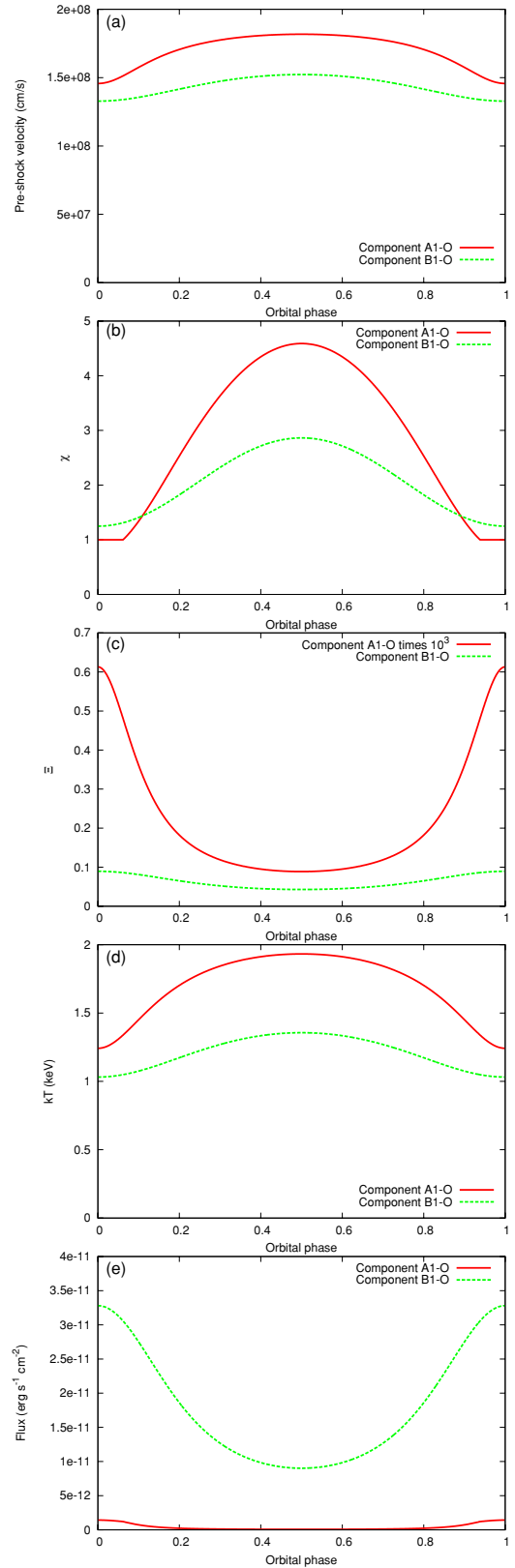


Figure 4. Variation with orbital phase of various parameters in the calculations of the X-ray luminosity generated in the multiple wind–wind collisions. From top left to bottom right: (a) pre-shock velocity, (b) cooling parameter χ , (c) fraction of wind kinetic power thermalized in the collision Ξ , (d) the mean post-shock temperature kT , and (e) the intrinsic X-ray flux due to wind–wind collisions from each component. χ 's are limited to 1 if the actual value is lower. The contributions from the post-shock gas of the different components are phased to their respective system, i.e., the contribution from component A1-O is phased to system A. Note that in the plot Ξ_{A1} has been multiplied by a factor of 10^3 for comparative purposes.

for sources which have been corrected only for ISM absorption. Coincidentally, the circumstellar absorption to the WCR between systems A and B is very small, so that this component essentially suffers only ISM absorption. The resulting attenuated spectra are displayed in the bottom panel of Figure 5. With the exception of the EWS emission, there is a consistent trend of a turnover energy of ~ 1 keV. Furthermore, the biggest victims of energy dependent absorption are components A1-O and B1-O, which can be seen from a comparison of the intrinsic and attenuated spectra in Figure 5.

4.3. Comparison to Observations

The model predictions and observations are in good agreement for a number of features. For instance, the X-ray emission from wind collision shocks can explain the hot plasma component derived from the spectral fits. Despite this, if all of the emitters in the system are active the total attenuated flux predicted by the model is ~ 10 – 20 times higher than the fluxes obtained from the spectral fits, with the dominant contribution to the model flux coming from the post-shock gas of component B1-O (see bottom panel of Figure 6). However, it is unclear whether the assumption of a normal wind for component B1-O is justified as Leung et al. (1979) suggested that this system is semi-detached. Numerical models of short period, massive star binary systems by Dessart et al. (2003) have shown that even a relatively small mass transfer rate ($\simeq 5 \times 10^{-6} M_{\odot} \text{ yr}^{-1}$) is unimpeded by the winds of the stars and can therefore disrupt the apex of the WCR. To gain a better agreement between the model and observations it would seem necessary for some mechanism to kill-off the X-ray emission from system B; mass transfer is a viable option.

Recalling that a comparison of the spectra from QZ Car and those of single and binary stars in Carina showed that on the basis of the spectral shape and the derived plasma temperatures we cannot directly infer the presence of wind–wind collision shocks, one may be inclined to neglect the MWC emission also. Yet, if we only consider the X-ray emission from the individual stars (hereafter Scenario 1) there is a deficit between model and observation of a factor of ~ 2 – 3 (see Figure 7).¹⁵ Including the MWC emission (hereafter Scenario 2) remedies the shortfall, and a good agreement is attained when stellar mass-loss rates are reduced by a factor of 1.1. Noting that massive star winds are inhomogeneous (see Puls et al. 2008, for a recent review), and that results from detailed observational studies suggest that previous mass-loss rate estimates (e.g., Howarth & Prinja 1989) require scaling down by factors of 2–5 (Bouret et al. 2003; Repolust et al. 2004; Markova et al. 2004; Fullerton et al. 2006; Moffat 2008; Waldron & Cassinelli 2010), this seems to be a reasonably modest alteration. Notwithstanding the improved agreement between the model and observed fluxes, the average column derived from the spectral fits ($\sim 0.2 \times 10^{22} \text{ cm}^{-2}$) is significantly higher than the value calculated for the MWC. This could be indicating two things. The first is that in using Equation (8) we may be underestimating the column density to the shocked gas between systems A and B, or that a more detailed description of the X-ray emission and absorption to the individual stars is warranted.

¹⁵ Our adopted stellar parameters (Table 2) lead to an integrated L_{bol} for QZ Car which is a factor of ~ 2 lower than determined by Povich et al. (2011). Although increasing L_{bol} by this factor will cause a corresponding increase in L_X , the shortfall between Scenario 1 and the observed fluxes in Figure 7 would not be remedied.

Bearing in mind that the X-ray flux from the MWC $\propto 1/d_{\text{sepA+B}}$ (since the shocked gas is adiabatic), we raise the question of whether a lower limit can be placed on $d_{\text{sepA+B}}$ if we make a slightly larger (but still reasonable) reduction in mass-loss rates? Proceeding with this approach the observed flux level can be approximately matched if we reduce \dot{M} 's by a factor of 3 and decrease $d_{\text{sepA+B}}$ to $6 \times 10^{13} \text{ cm}$, i.e., a factor of 10 smaller than the upper limit given by Nelan et al. (2004). This alternation in fact causes a negligible change to the column density calculated for the MWC. However, due to the uncertainty in the orbital eccentricity of system AB this is a somewhat tentative lower limit.

5. DISCUSSION

The presence of a hot plasma component with $kT \simeq 2$ keV in the spectral fits could be providing evidence for wind–wind collision shocks in QZ Car. However, to prevent our model predictions from considerably overestimating the observed flux we must suppress the prominent X-ray emission from system B. This is an interesting result as mass transfer in system B could provide an effective mechanism to disrupt the WCR, and therefore our results support the previous suggestion by Leung et al. (1979) of mass transfer in system B (see also Morrison & Conti 1980). Reassuringly, this result is unaffected by our adopted distance to QZ Car—we adopt a distance of 2.3 kpc which differs from that of Southworth & Clausen (2007) who quote a value of 2.8 kpc. The net effect of using this slightly larger distance would be a reduction in the calculated fluxes by a factor of ~ 0.67 , which would not affect our qualitative conclusions. We must note, however, that although additional emission from the MWC is required in our model, a more detailed description of the emission from the single star than adopted in this work may render this unnecessary. Furthermore, the ISM column density provides the dominant absorption to the MWC and the individual stars, therefore, a small increase/decrease in the ISM column could have implications for our model results.

This semi-analytical model has nevertheless provided a great deal of insight. Further progress will require detailed hydrodynamical modeling which should consider the following factors.

1. The stellar separations in the binary systems are relatively small and therefore the interaction between the stellar radiation fields may affect the wind acceleration (e.g., inhibition or braking; Stevens & Pollock 1994; Gayley et al. 1997) which would alter the resulting X-ray flux (e.g., Parkin et al. 2009).
2. Post-shock gas is in reality multi-temperature and more accurate comparisons against the observed spectra will require this to be taken into account.
3. The nature of system B must be properly considered.
4. We account for the radiative behavior of the shocked gas through the $1/\chi$ scaling in Equation (1). However, the effect of radiative cooling on the dynamics and the X-ray emission is likely to be more complicated (e.g., Stevens et al. 1992; Myasnikov et al. 1998; Antokhin et al. 2004; Pittard 2009; Parkin & Pittard 2010; Parkin et al. 2010).
5. Contrasting views exist as to the X-ray generation mechanism for single O-type stars. For instance, recent high resolution analysis of O-type stars has given evidence for a decrease in X-ray temperature in the stellar wind as one tends to larger radii (Waldron & Cassinelli 2007). This poses questions for the classic picture of X-ray generation

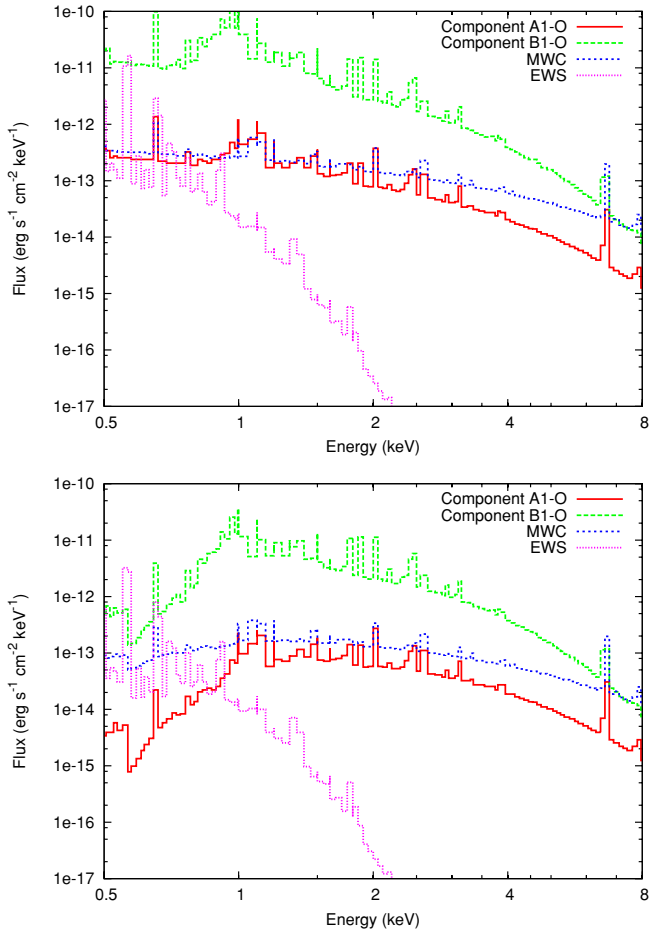


Figure 5. Intrinsic (top panel) and attenuated (bottom panel) synthetic 0.5–8 keV X-ray spectra for ObsID 6402.

by instability driven shocks, whereby higher X-ray temperatures are attained at larger radii at which point the flow has been accelerated somewhat (Owocki et al. 1988). Thus, it would be appropriate to assess these models in future work, in particular examining the spatial and energy dependence of the X-ray emission and absorption (e.g., Leutenegger et al. 2010).

6. CONCLUSIONS

We have presented a series of nine observations of the multiple star system QZ Car obtained with *Chandra* over a period of roughly 2 years. The spectral fits are characterized by cool, moderate, and hot temperature plasma components at $kT \simeq 0.2, 0.7,$ and 2 keV, respectively, a circumstellar absorption of $\simeq 0.2 \times 10^{22} \text{ cm}^{-2}$, and an average flux of $\simeq 7 \times 10^{-13} \text{ erg s}^{-1} \text{ cm}^{-2}$. There appears to be no clear correlation between the fluxes and the orbits of the constituent binaries. The most compelling evidence for any correlation is between the high temperature thermal plasma component and the orbit of the O9.7 I + b2 v binary (system A), although due to limited statistics the high temperature plasma component is poorly constrained. Curiously, there is also a deficit between the X-ray flux expected from the single stars and that derived from the spectral fits.

A semi-analytical model of QZ Car was constructed. A stable momentum balance is not attained between the winds in either the O9.7 I + b2 v binary (system A) or the O8 III + o9 v binary (system B), and despite possessing the strongest stellar wind in

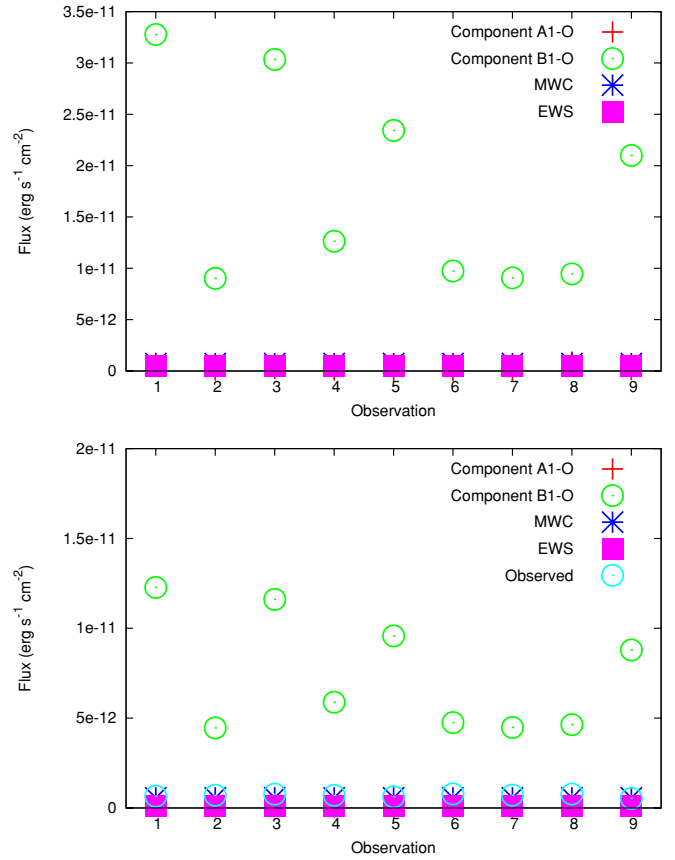


Figure 6. Variation of the intrinsic (top panel) and attenuated (bottom panel) X-ray fluxes from wind–wind collisions. The fluxes are integrated from the synthetic spectra in the 0.5–8 keV range. The observed fluxes are also plotted for comparison (see Table 4). Clearly, if one sums the contributions from all of the emitters in the model the flux exceeds the observed values derived from the spectral fits. Note the difference in scale between the plots.

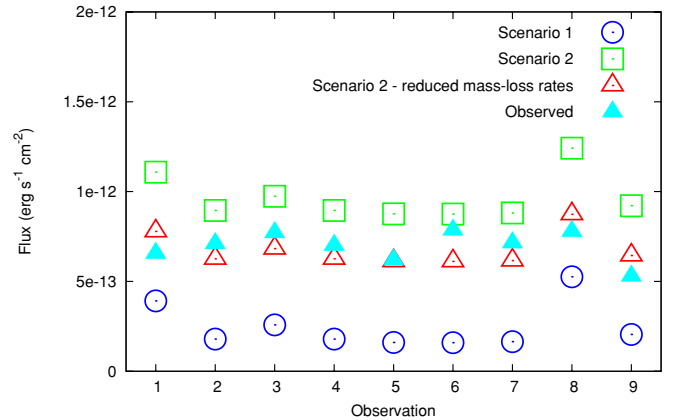


Figure 7. Integrated 0.5–8 keV fluxes predicted by the model compared against the values attained from the spectral fits.

QZ Car the O9.7 I star is a weak emitter (in terms of wind–wind collision emission) due to the relatively small fraction of its wind being shocked. The higher fraction of the primary star’s wind being shocked in the O8 III + o9 v binary (system B) makes it the dominant emitter, although the magnitude of its X-ray emission exceeds the flux level derived from the spectral fits by more than a factor of 10. The necessity of a disrupted WCR in the O8 III + o9 v binary to bring the model results

and observations into better agreement gives some compelling evidence in support of Leung et al. (1979)'s suggestion of mass transfer.

We conclude that the magnitude and lack of variability in the fluxes derived from the spectral fits can be well matched by a combination of X-ray emission from the individual stars and the mutual wind–wind collision between the two binary systems, albeit with stellar wind mass-loss rates reduced in line with the current consensus for inhomogeneous winds. The observed column density is, however, not well matched by the model. This may be indicating that a more complex prescription for the emission from the individual stars is required, or also that the column density calculation is not completely appropriate for the mutual wind–wind collision between the two binary systems. Our analysis places a somewhat tentative lower limit on the separation of the two binary systems of $\simeq 7$ AU.

Future analysis would benefit from further observations. A follow-up X-ray observation with significant enough exposure time to allow a satisfactory fit with a three-temperature plasma model with discrete absorption components could constrain the column density to the hot plasma. At radio wavelengths it may in fact be possible to resolve the separate emission peaks (e.g., Dougherty et al. 2005). However, the sensitivity of current instruments would require a long observation to attain sufficient statistics, which considering the timescale of the binary orbits may cause detailed structure to become smeared (Pittard 2010). With our results providing support for mass transfer in the O8 III + o9 v binary, multi-wavelength observations may reveal a far more complicated picture for QZ Car (e.g., β Lyrae; Ignace et al. 2008).

We thank Rodolfo Barbá and the OWN Team (Barbá et al. 2010) for providing new high-resolution optical spectroscopic results in advance of publication, Nolan Walborn for deriving new spectral classifications from those data, as well as for useful discussions, and the referee for a helpful and insightful report. E.R.P. was supported in part by a Henry Ellison Scholarship from the University of Leeds, and by a PRODEX XMM/Integral contract (Belpo). E.R.P. also thanks Penn State University for their hospitality during a fruitful visit. J.M.P. gratefully acknowledges funding from the Royal Society. A.F.J.M. is grateful for financial assistance from NSERC (Canada) and FQRNT (Quebec). Y.N. acknowledges support from the Fonds National de la Recherche Scientifique (Belgium), the PRODEX XMM and Integral contracts, and the “Action de Recherche Concertée” (CFWB-Académie Wallonie Europe). W.L.W. acknowledges partial support from *Chandra* grant AR8-9003A. This work is supported by *Chandra X-ray Observatory* grant GO8-9131X (PI: L. Townsley) and by the ACIS Instrument Team contract SV4-74018 (PI: G. Garmire), issued by the *Chandra X-ray Center*, which is operated by the Smithsonian Astrophysical Observatory for and on behalf of NASA under contract NAS8-03060.

Note added in proof. In October 2010, just before this paper was submitted, the *Chandra X-ray Center* announced the discovery of a hook-shaped feature in the *Chandra* PSF¹⁶, extending $\sim 0''.8$ from the main peak and containing $\sim 5\%$ of the flux. The validity of up to 18 of the $> 14,000$ CCCP point sources ($\sim 0.1\%$) may be called into question due to this PSF feature. Those sources are flagged in the “CCCP X-ray Sources and Properties” table in Broos et al. (2011).

REFERENCES

- Allen, D. A., & Hillier, D. J. 1993, *Proc. Astron. Soc. Aust.*, **10**, 338
 Anders, E., & Grevesse, N. 1989, *Geochim. Cosmochim. Acta*, **53**, 197
 Antokhin, I. I., Owocki, S. P., & Brown, J. C. 2004, *ApJ*, **611**, 434
 Arnaud, K. A. 1996, in ASP Conf. Ser. 101, *Astronomical Data Analysis Software and Systems V*, ed. G. H. Jacoby & J. Barnes (San Francisco, CA: ASP), 17
 Barbá, R. H., Gamén, R., Arias, J. I., Morrell, N., Maíz Apellániz, J., Alfaro, E., Walborn, N., & Sota, A. 2010, *RevMexAA Ser. Conf.*, **38**, 30
 Bouret, J., Lanz, T., Hillier, D. J., Heap, S. R., Hubeny, I., Lennon, D. J., Smith, L. J., & Evans, C. J. 2003, *ApJ*, **595**, 1182
 Broos, P., Townsley, L., Getman, K., & Bauer, F. 2002, ACIS Extract, An ACIS Point Source Extraction Package, Pennsylvania State University, http://www.astro.psu.edu/xray/docs/TARA/ae_users_guide.html
 Broos, P. S., Feigelson, E. D., Townsley, L. K., Getman, K. V., Wang, J., Garmire, G. P., Jiang, Z., & Tsuboi, Y. 2007, *ApJS*, **169**, 353
 Broos, P. S., Townsley, L. K., Feigelson, E. D., Getman, K. V., Bauer, F. E., & Garmire, G. P. 2010, *ApJ*, **714**, 1582
 Broos, P. S., et al. 2011, *ApJS*, **194**, 2 (CCCP Catalog Paper)
 Chlebowski, T., & Garmany, C. D. 1991, *ApJ*, **368**, 241
 Cox, A. N. (ed.) 2000, *Allen's Astrophysical Quantities* (4th ed.; New York: AIP)
 Davis, J. E. 2001, *ApJ*, **562**, 575
 De Becker, M., Rauw, G., Blomme, R., Pittard, J. M., Stevens, I. R., & Runacres, M. C. 2005, *A&A*, **437**, 1029
 Dessart, L., Langer, N., & Petrovic, J. 2003, *A&A*, **404**, 991
 Dougherty, S. M., Beasley, A. J., Claussen, M. J., Zauderer, B. A., & Bolingbroke, N. J. 2005, *ApJ*, **623**, 447
 Ferland, G. J. 2000, *RevMexAA Ser. Conf.*, **9**, 153
 Ferland, G. J., Korista, K. T., Verner, D. A., Ferguson, J. W., Kingdon, J. B., & Verner, E. M. 1998, *PASP*, **110**, 761
 Fullerton, A. W., Massa, D. L., & Prinja, R. K. 2006, *ApJ*, **637**, 1025
 Gayley, K. G., Owocki, S. P., & Cranmer, S. R. 1997, *ApJ*, **475**, 786
 Herbst, W. 1976, *ApJ*, **208**, 923
 Howarth, I. D., & Prinja, R. K. 1989, *ApJS*, **69**, 527
 Ignace, R., Oskinova, L. M., Waldron, W. L., Hoffman, J. L., & Hamann, W. 2008, *A&A*, **477**, L37
 Kaastra, J. S. 1992, Internal SRON-Leiden Report
 Leung, K.-C., Moffat, A. F. J., & Seggewiss, W. 1979, *ApJ*, **231**, 742
 Leutenegger, M. A., Cohen, D. H., Zsargó, J., Martell, E. M., MacArthur, J. P., Owocki, S. P., Gagné, M., & Hillier, D. J. 2010, *ApJ*, **719**, 1767
 Markova, N., Puls, J., Repolust, T., & Markov, H. 2004, *A&A*, **413**, 693
 Martins, F., Schaerer, D., & Hillier, D. J. 2005, *A&A*, **436**, 1049
 Mason, B. D., Gies, D. R., Hartkopf, W. I., Bagnuolo, W. G., Jr., ten Brummelaar, T., & McAlister, H. A. 1998, *AJ*, **115**, 821
 Mayer, P., Lorenz, R., Drechsel, H., & Abseim, A. 2001, *A&A*, **366**, 558
 Mayer, P., Niarchos, P. G., Lorenz, R., Wolf, M., & Christie, G. 1998, *A&AS*, **130**, 311
 Mewe, R., Kaastra, J. S., & Liedahl, D. A. 1995, *Legacy*, **6**, 16
 Moffat, A. F. J. 2008, in *Clumping in Hot-Star Winds*, ed. W.-R. Hamann, A. Feldmeier, & L. M. Oskinova (Potsdam: Univ. Potsdam), 17
 Morrison, N. D., & Conti, P. S. 1979, in *IAU Symp. 83, Mass Loss and Evolution of O-Type Stars*, ed. P. S. Conti & C. W. H. de Loore (Cambridge: Cambridge Univ. Press), 277
 Morrison, N. D., & Conti, P. S. 1980, *ApJ*, **239**, 212
 Myasnikov, A. V., Zhekov, S. A., & Belov, N. A. 1998, *MNRAS*, **298**, 1021
 Nazé, Y. 2009, *A&A*, **506**, 1055
 Nazé, Y., et al. 2011, *ApJS*, **194**, 7 (CCCP Massive Star Lx/Lbol Paper)
 Nelan, E. P., Walborn, N. R., Wallace, D. J., Moffat, A. F. J., Makidon, R. B., Gies, D. R., & Panagia, N. 2004, *AJ*, **128**, 323
 Oskinova, L. M. 2005, *MNRAS*, **361**, 679
 Owocki, S. P., Castor, J. I., & Rybicki, G. B. 1988, *ApJ*, **335**, 914
 Owocki, S. P., & Cohen, D. H. 1999, *ApJ*, **520**, 833
 Parkin, E. R., & Pittard, J. M. 2008, *MNRAS*, **388**, 1047
 Parkin, E. R., & Pittard, J. M. 2010, *MNRAS*, **406**, 2373
 Parkin, E. R., Pittard, J. M., Corcoran, M. F., & Hamaguchi, K. 2011, *ApJ*, **726**, 105
 Parkin, E. R., Pittard, J. M., Corcoran, M. F., Hamaguchi, K., & Stevens, I. R. 2009, *MNRAS*, **394**, 1758
 Pittard, J. M. 2009, *MNRAS*, **396**, 1743
 Pittard, J. M. 2010, *MNRAS*, **403**, 1633
 Pittard, J. M., & Parkin, E. R. 2010, *MNRAS*, **403**, 1657
 Pittard, J. M., & Stevens, I. R. 1997, *MNRAS*, **292**, 298
 Pittard, J. M., & Stevens, I. R. 2002, *A&A*, **388**, L20
 Pollock, A. M. T. 1987, *ApJ*, **320**, 283
 Povich, M. S., et al. 2011, *ApJS*, **194**, 6 (CCCP Massive Star Candidates Paper)

¹⁶ http://cxc.harvard.edu/ciao/caveats/psf_artifact.html

- Prinja, R. K. 1989, *MNRAS*, [241](#), [721](#)
- Puls, J., Vink, J. S., & Najarro, F. 2008, *A&AR*, [16](#), [209](#)
- Repolust, T., Puls, J., & Herrero, A. 2004, *A&A*, [415](#), [349](#)
- Smith, N. 2002, *MNRAS*, [337](#), [1252](#)
- Smith, N. 2006, *MNRAS*, [367](#), [763](#)
- Smith, R. K., Brickhouse, N. S., Liedahl, D. A., & Raymond, J. C. 2001, *ApJ*, [556](#), [L91](#)
- Southworth, J., & Clausen, J. V. 2007, *A&A*, [461](#), [1077](#)
- Stevens, I. R., Blondin, J. M., & Pollock, A. M. T. 1992, *ApJ*, [386](#), [265](#)
- Stevens, I. R., & Pollock, A. M. T. 1994, *MNRAS*, [269](#), [226](#)
- Townsley, L. K., Broos, P. S., Feigelson, E. D., Garmire, G. P., & Getman, K. V. 2006, *AJ*, [131](#), [2164](#)
- Townsley, L. K., et al. 2011, *ApJS*, [194](#), 1 (CCCP Intro Paper)
- Vink, J. S., de Koter, A., & Lamers, H. J. G. L. M. 2000, *A&A*, [362](#), [295](#)
- Walborn, N. R. 1995, *RevMexAA Ser. Conf.*, [2](#), [51](#)
- Waldron, W. L., & Cassinelli, J. P. 2007, *ApJ*, [668](#), [456](#)
- Waldron, W. L., & Cassinelli, J. P. 2010, *ApJ*, [711](#), [L30](#)
- Wilms, J., Allen, A., & McCray, R. 2000, *ApJ*, [542](#), [914](#)